

Article

Superhydrophobic Surface with Gamma Irradiation Resistance and Self-Cleaning Effect in Air and Oil

Yan Zhang * , Jing Zhang and Yujian Liu

Key Laboratory of Specially Functional Polymeric Materials and Related Technology (ECUST), Ministry of Education, School of Materials Science and Engineering, East China University of Science and Technology, MeiLong Road 130, Shanghai 200237, China; 13162216896@163.com (J.Z.); yjliu@ecust.edu.cn (Y.L.)

* Correspondence: yzhang@ecust.edu.cn

Received: 9 December 2019; Accepted: 23 January 2020; Published: 26 January 2020



Abstract: A superhydrophobic surface was synthesized by a combination of an epoxy/polymethylphenylsiloxane matrix and dual-scale morphology of silica (SiO₂) nanoparticles. When the amount of SiO₂ reached 30 wt.%, the as-prepared surface showed a high static water contact angle (WCA) of 154° and a low sliding angle (SA) of 5°, excellent water repellency, and dirt-removal effects both in air and oil (hexamethylene). Even after exposure to as high as a 12.30 Mrad dose of gamma-rays, the composite surface still maintained its superior performance.

Keywords: epoxy resin; superhydrophobic; self-cleaning; gamma irradiation resistance

1. Introduction

Nuclear energy is an attractive solution for electricity demand due to its high efficiency and is carbon-neutral [1]. Nevertheless, the disasters that occurred at Fukushima (Japan, 2011) [2], Chernobyl (Ukraine, 1986) [3], and Three Mile Island (USA, 1979) [4] have aroused considerable concern regarding their safety. One of the severe environmental consequences of these nuclear accidents is the enormous fallout of long-lived and highly radioactive substances such as I-137, Cs-137, Xe-133, and so on. For example, the total amount of radioactivity released from the nuclear fuel into the environment at the Three Mile Island accident was about 9.25×10^{16} Bq, of which about 60% was Xe-133, and 5.55×10^{11} Bq was I-137 [5], whereas the Chernobyl accident reached 1.7×10^{18} Bq [6], and the I-137 and Cs-137 leakages during the Fukushima accident were about 1.5×10^{17} and 1.21×10^{16} Bq, respectively [7]. These contaminations would be adsorbed and retained on the surface of the wall and equipment for a very long time [2], and even as secondary pollution carried out with mobile devices like the rescue robot. Surfaces with superior self-cleaning properties are an effective solution for those challenging problems. However, as we know, most polymers are susceptible to gamma irradiation. High energy and high dose radiation usually cause chain-scission and free radical-recombination, which further leads to cracking as well as the apparent degradation of the mechanical strength of the coatings [8,9].

Superhydrophobic surfaces, inspired by the natural lotus, have gained an intense interest in recent years [10–12]. Many technologies including lithography [13], electrospinning [14], template [15], anodic oxidation [16], and electrochemical deposition [17] have been utilized in this field. For instance, Shieh fabricated a robust air like superhydrophobic surfaces with a combination of e-beam lithography, dry etching, the hydrogen plasma etching approach, and then hydrophobized with CHF₃ plasma [18]. The two-tier air-like structures consisted of nanopillars and nanograss, and over 99.9% of the surface was composed of air. Therefore, the static water contact angle (WCA) of the surface was close to 180°, and the sliding angle (SA) was close to 0°. A superhydrophobic polydimethylsiloxane/poly (methyl methacrylate) (PDMS/PMMA) membrane was achieved by using the electrospinning method [19]. However, a big challenge in their application is poor mechanical stability, where most would lose

function when exposed to oil as the low surface tension of the oil makes it easy to penetrate through the surfaces [20]. Additionally, the weak or uncrosslinked chemical bonds of low surface energy substances like alkane, silicone, and fluoride usually lead to poor UV durability as well as low resistance to corrosive liquids and organic solvents [21]. In contrast, epoxy resins as well as its composites have been widely employed in severe environments such as marine-varnishes, and chemical and nuclear plant surfaces due to their excellent adhesion, mechanical properties, and good solvent and chemical resistance [22–25]. Furthermore, the abundant hydroxyl and epoxy groups also result in high surface energy.

In consideration of complex and hostile nuclear circumstances, for instance, salted or acid liquids, solid dust or greasy dirt [26], especially with extreme high energy gamma irradiation, bisphenol-A epoxy resin (E-51) was selected as the matrix of the surfaces and hydroxyl-terminated polymethylphenylsiloxane (HT-PMPS) with high hydrophobicity was copolymerized with E-51 resins to obtain low surface energy. Furthermore, the dual-scale rough silica particles prepared by the sol-gel method were applied to construct micro/nano hierarchical morphology. The wettability, self-cleaning effect, and gamma irradiation stability of the as-prepared surfaces were then further investigated.

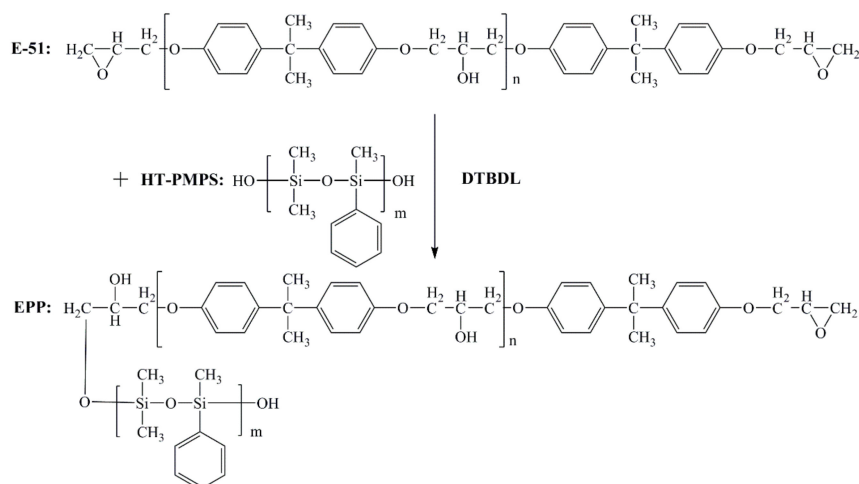
2. Materials and Methods

2.1. Materials

Epoxy resin (diglycidyl ether of bisphenol A, E-51), with an epoxide number of 0.508 and dynamic viscosity of 12,000~14000 mPa·s, was purchased from Shanghai Huayi Resin Co. Ltd. (Shanghai, China). Isophorone diamine, dibutyltindilaurate (DTBDL), and SiO₂ (99.5%, metals basis) with an average particle size of 15 nm were provided by Aladdin Biochemical Reagent Co. Ltd. (Shanghai, China). Other analytically pure chemicals including alcohol, hexamethylene, tetraethylorthosilicate (TEOS), and saturated ammonium hydroxide solution (26%–28%) were received from Shanghai Lingfeng Reagent Co. Ltd. (Shanghai, China). Dow Corning provided hydroxyl-terminated polymethylphenylsiloxane (HT-PMPS) with a specific gravity of 1.07 and viscosity of 10~30 mPa·s.

2.2. Synthesis of Polymethylphenylsiloxane-Modified Epoxy Resin

Epoxy resin and hydroxyl-terminated polymethylphenylsiloxane were added into a three-necked flask together with dibutyltindilaurate as the catalyst, and the reaction was carried out at 90 °C for 3 h. The molar ratio of E-51 and HT-PMPS is 6:4. Then, a viscous silicone-modified epoxy resin (EPP) was obtained, as sketched in Scheme 1.



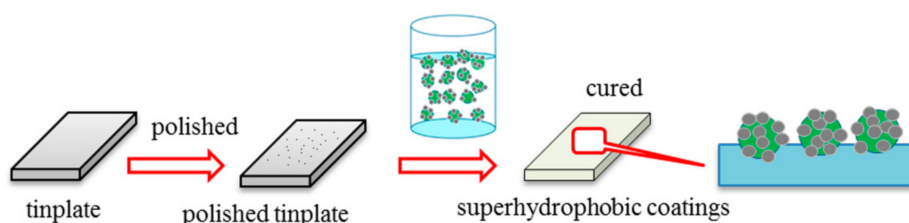
Scheme 1. Synthesis of the silicone-modified epoxy resin.

2.3. Preparation of Dual-Scale Silica Particles

The large silica nanoparticles were prepared by following Stöbe methods, and ammonium hydroxide was used as the catalyst [27]. A total of 3 mL tetraethylorthosilicate (TEOS), 45 mL alcohol, and 8 mL ammonium hydroxide solution (26%–28%) was added, in succession, in a three-neck flask and stirred at 50 °C for 1 h. Then, small SiO₂ (15 nm) particles were added to the solution and stirred for 3 h. After centrifugation, dual-scale rough silica particles were obtained.

2.4. Fabrication of Superhydrophobic Surface

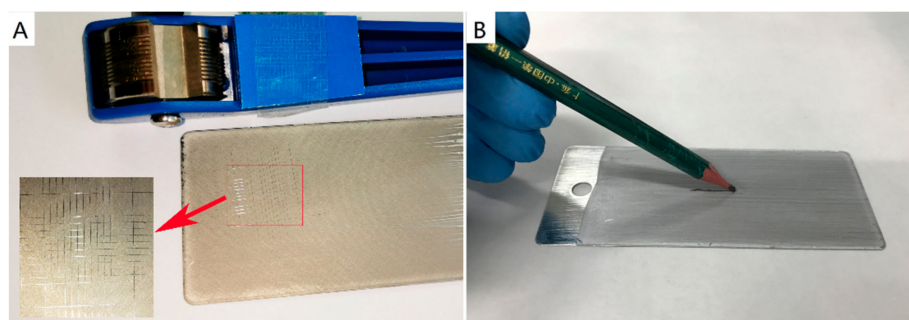
The as-prepared dual-scale silica particles were first ultrasonically dispersed in 25 mL xylene and then mixed with silicone-modified epoxy resins and a curing agent of isophorone diamine. After roller coating with a drawdown bar, the surfaces with a thickness of 25 μm were cured at 80 °C for 4 h and 120 °C for 1 h. The obtained surfaces were denoted as EPPS-x, where x is the mass fraction of SiO₂. The whole process is illustrated in Scheme 2.



Scheme 2. Fabrication of the superhydrophobic surface.

2.5. Characterization

Fourier transform infrared (FTIR) spectroscopy was conducted on a Nicolet 5700 (Thermo, Waltham, MA, USA) from 4000–400 cm⁻¹. Epoxide equivalent weight (EEW) of the modified resins was determined according to the GB/T 1677–2008 standards [28]. Transmission electron microscopy (TEM) was performed with a JEM-1400 TEM (JEOL, Tokyo, Japan). Morphologies of the surfaces were examined with field emission scanning electron microscopy (FESEM, S4800, Hitachi, Tokyo, Japan). Dynamic light scattering (DLS) was conducted on a Malvern Zetasizer nano HT system. The roughness was measured by an atomic force microscope (AFM, DI, Veeco, New York, NY, USA) with a scanning area of 20 μm × 20 μm and a scanning rate of 0.5003 Hz. The roughness value was an average measurement with a scanning number of 256. The static water contact angle and sliding angle were carried out on contact angle meters (JC2000D2 and JC2000D3, Powereach, Shanghai, China) with water droplets of 5 μL. At least three points were measured at different locations of the samples to provide the data. The adhesion and hardness of the surfaces were evaluated, refereeing ASTM D3359-09 [29] and ASTM D3363-00 standards [30], respectively, as displayed in Scheme 3. The tests were conducted as follows. A lattice pattern was made in the surface, then pressure-sensitive tape was applied over the lattice and then removed, followed by an assessment of the adhesion of the surface qualitatively on a 0 to 5 scale. A pencil lead, made by Chunghwa, China First Pencil Co. Ltd., with a defined geometry, was pushed over the surface at an angle of 45°. The hardness of the pencil lead was increased in steps until visible defects marked the surface. Water droplets were dropped on the slant (6°) sample with graphite powder placed evenly to observe the self-cleaning effect of the surfaces [21].



Scheme 3. (A) Adhesion, and (B) hardness tests of the samples.

2.6. Irradiation

In some harsh nuclear accidents, a radiation dose may increase to 10^5 – 10^6 rad. The surfaces were irradiated at the Co-60 gamma-ray facility (from Institute of Nuclear Technology Application, ECUST) with a dose rate of 0.98×10^5 , 1.81×10^5 , 2.66×10^5 , 6.01×10^5 , and 1.45×10^6 rad/h, respectively, for 8.5 h under an air environment and room temperature, as shown in Figure 1. The radiation dose rate was corrected by using the potassium dichromate chemical method [31]. Cr^{6+} is reduced to Cr^{3+} under irradiation, resulting in the change of absorbance. The gamma radiation dose rate can be calculated according to the change of absorbance. Additionally, the radiation dose rate was calibrated by the Shanghai Institute of Measurement and Testing Technology. The total radiation doses were 0.83, 1.54, 2.26, 5.11, and 12.30 Mrad, respectively.

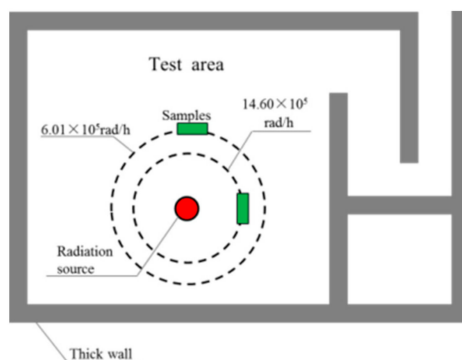


Figure 1. Irradiation chamber and specimen geometry.

3. Results and Discussions

3.1. Silicone Modified Epoxy Resin

The FTIR spectra of the bisphenol-A epoxy resin (E-51), hydroxyl-terminated polymethylphenylsiloxane (HT-PMPS), and modified epoxy resin (EPP) are shown in Figure 2. The characteristic absorption peaks at 1429 cm^{-1} and 1265 cm^{-1} can be attributed to the methyl group stretching of $\text{Si-C}_6\text{H}_5$ and Si-CH_3 , respectively. After the reaction of E-51 and HT-PMPS, a new peak at around 1128 cm^{-1} appeared, indicating the formation of the Si-O-C bond. However, the overlap of the Si-O-C characteristic peak with the Si-O-Si peak in the region of 1081 – 1132 cm^{-1} made it difficult to observe, and the peak became broader after the reaction. Furthermore, the epoxide number of EPP decreased from 0.508 (E-51) to 0.382, also suggesting a partial reaction between two resins.

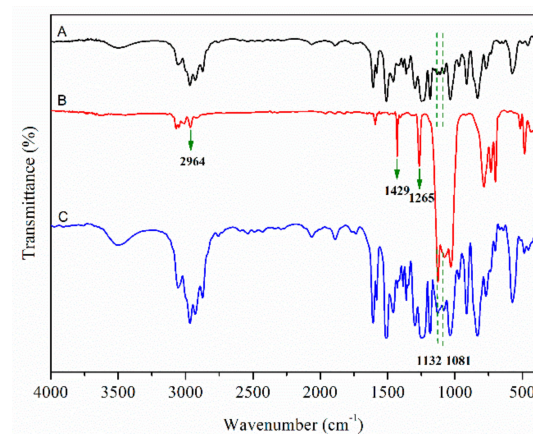


Figure 2. Fourier Transform Infrared (FTIR) spectra of (A) epoxy resin (E-51), (B) hydroxyl-terminated polymethylphenylsiloxane (HT-PMPS), and (C) silicone-modified epoxy resins (EPP).

3.2. Dual-Scale Silica Particles

The average size of the as-prepared large silica particles measured by the DLS was 900 nm, and the result is shown in Figure 3. The small silica particles (15 nm) were covalently grafted onto the large ones via the condensation reaction between the hydroxyl groups, giving rise to a dual-scale hierarchical morphology, as displayed in Figure 4. As abundant air pockets are easily confined by this kind of dual-scale structure, the water droplet can sit on the layer of air, leading to a superhydrophobic surface [32]. Furthermore, the dual-scale hierarchical structure of silica particles exhibits high stability in a hot and humid environment [33].

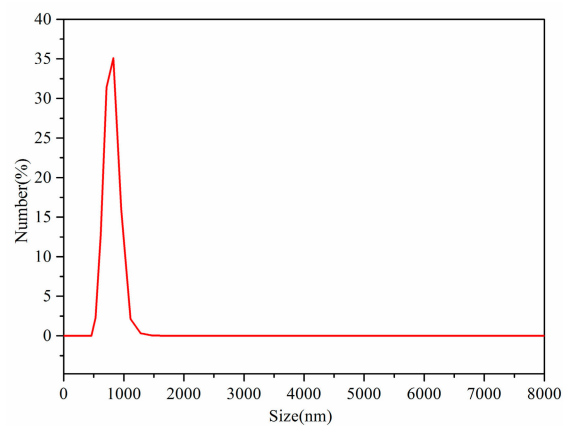


Figure 3. Size distribution of large silica nanoparticles.

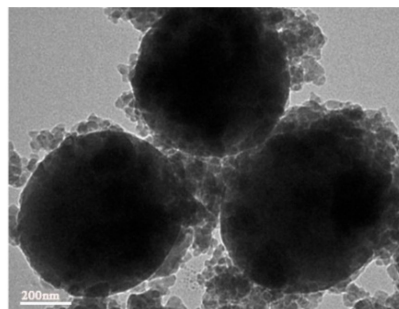


Figure 4. The transmission electron microscopy (TEM) image of the as-prepared composite silica particles.

3.3. Static Water Contact Angle of the Surfaces

The static water contact angles (WCA) and sliding angles (SA) of the surfaces are illustrated in Figure 5. With the enhancement of the silica particle concentration, the static contact angle of the samples increased, and the sliding angle decreased. The high WCA (154°) and low SA (5°) of EPPS-30 demonstrated that the super hydrophobicity was achieved by the combination of the low surface energy of the silicone-modified epoxy resin and dual-scale hierarchical structure.

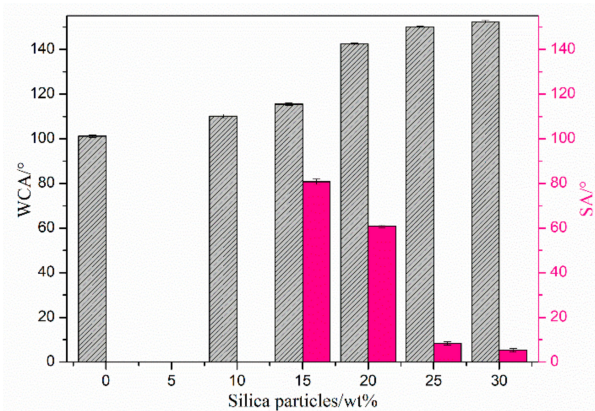


Figure 5. Static water contact angle (WCA) and sliding angle (SA) of the surfaces with different content of silica particles.

3.4. Morphology and Roughness of the Surfaces

The morphologies of the surfaces with different amounts of dual-scale silica particles are presented in Figure 6, and the roughness characterized by the atomic force microscope (AFM) was listed in Table 1. All samples possessed a micro/nano hierarchical structure. However, when the content of silica particles was less than 15 wt.%, the substrate was only partly coated by the particles (Figure 6A1), and the roughness of the surface (R_q) was only 240 nm, which was much lower than others. In this specific case, the cavity between the particles was too wide to hold air pockets, so its static water contact angle was only 101°. As the content of the particles increased, the substrate was gradually covered by more and more micro/nano bumps of silica particles. As the roughness of the surface increased, more air pockets could be trapped in the interstices. When the amount of silica particles reached 30 wt.%, the WCA of the surface rose to 154°, and the sliding angle dropped to 5°, implying its superhydrophobicity. While further raising the silica content to 35 wt.%, the particles could be easily erased from the surface for lack of a sufficient resin coating and the performance of the surface declined significantly.

Table 1. The average roughness of the surfaces with different contents of silica particles.

Sample	EPPS10	EPPS15	EPPS20	EPP25	EPP30
R_q (nm)	240	267	416	480	726
R_a (nm)	188	207	335	505	526

3.5. Self-Cleaning Effect

Graphite powder was used to simulate the removal process of radioactive dust. As water droplets fell onto the surface, they formed spherical shapes and rolled freely. Then, the rolling motion picked up and removed the dust very easily [20], as shown in Figure 7A–C.

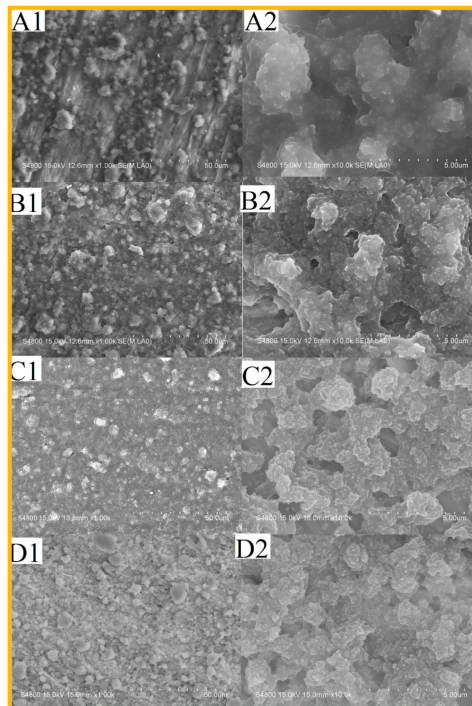


Figure 6. Scanning electron micrographs of the surfaces with different contents of silica particles viewed at 1000 \times magnification. (A1) 15 wt.%, (B1) 20 wt.%, (C1) 25 wt.%, (D1) 30 wt.%, and 10,000 \times magnifications (A2) 15 wt.%, (B2) 20 wt.%, (C2) 25 wt.%, (D2) 30 wt.%.

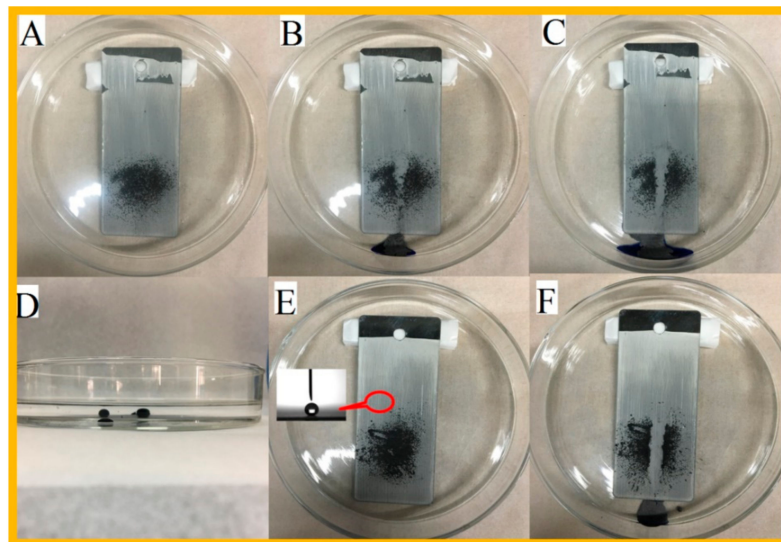


Figure 7. Self-cleaning test in air and oil. (A) The surface was covered by graphite, (B,C) process of self-cleaning in air, (D) water droplet was repelled by the surface in oil (hexamethylene), (E,F) the surface after being contaminated by oil without further water rinse.

Superhydrophobicity as well as the self-cleaning properties of surfaces might be destroyed when exposed to organic contaminants [34]. Due to the lower surface tension, it is much easier for oil to penetrate through the surfaces than the water. Usually, the weak bonding between the matrix and nanoparticles of the superhydrophobic surface results in the loss of water repellency even if partly contaminated by oil [35]. Epoxy resin, with strong adhesive strength, superior solvent and chemical resistance, can prevent oil from penetrating the surface effectively. Moreover, the dual-scale

structure of the silica nanoparticles allows more air pockets to exist between the water droplet and the solid surface [36]. In the Cassie state, the entrapped air plays an essential role in determining the superhydrophobicity of rough surfaces [37]. The contact area of the liquid and solid surface reduced sharply with air infusing into the rough surface [38]. When the as-prepared surface was immersed in oil, only a tiny amount of oil could penetrate the surface gradually, and the water droplets were supported by both the oil and the air pockets [39]. Therefore, the water droplets remained their “globularity” on the surface when immersed in oil (hexamethylene), and their WCA remained about 153° after immersion without further water rinse, as presented in Figure 7D–E. This shows that the surfaces maintain their water repellency and dirt-removal properties both in air and oil.

3.6. Gamma Irradiation Resistance

After as high as a 12.30 Mrad dose of gamma irradiation, the surfaces still exhibited satisfactory performance of high static WCA (152°), adhesion (5B), and pencil hardness (6H), as listed in Table 2. This can be attributed to the high radiation stability of the epoxy resin and the robust dual-scale structure of the as-prepared surfaces. In general, gamma irradiation causes the weak chemical bonds of resins to be broken and produce new free radicals [40]. Under low dose irradiation, chain crosslinking is the dominant reaction [41], which gives the surface a higher mechanical property and better thermal stability [42]. While further increasing the radiation dose, the performance of the materials deteriorated drastically because of the rapid chain degradation reaction. Our previous studies suggested that the gamma resistance of the polymer enhanced with the increase of the crosslink density [25,41]. The compact three-dimension network structure of epoxy resin is conducive to improving radiation stability. Furthermore, benzene rings of epoxy resin and polymethylphenylsiloxane are very stable under high irradiation dose and the sp^2 carbons of the benzene rings can also absorb the free radicals, thus slowing down the aging rate of the resins [23]. The adhesion and hardness of the surfaces are mainly dependent on the matrix itself. Epoxy resins modified with HT-PMPS exhibited superior gamma-ray stability. Therefore, even after 8.5 h of high dose rate gamma radiation, the surface remained superhydrophobicity, high adhesion, and hardness.

Table 2. Properties of the superhydrophobic surface after gamma irradiation.

Radiation Dose (Mrad)	0.83	1.54	2.26	5.11	12.30
Static contact angle (°)	152 ± 0.3	152 ± 0.6	153 ± 0.6	153 ± 0.5	152 ± 0.3
Adhesion	5B	5B	5B	5B	5B
Hardness	6H	6H	6H	6H	6H

4. Conclusions

A superhydrophobic composite surface was prepared with a combination of an epoxy/polymethylphenylsiloxane matrix and a dual-scale hierarchical morphology of silica nanoparticles. As the silica nanoparticle content increased from 10 to 30 wt.%, the roughness (R_q) of the surfaces rose from 240 nm to 726 nm, and the WCA increased from 101° to 154° accordingly. The results of the self-cleaning test suggest that the surface maintains water repellency when exposed to both air and oil (hexamethylene). Furthermore, the surface retains the superior performance of high WCA (152°), adhesion (5B), and hardness (6H) even after a 12.30 Mrad dose of gamma irradiation, indicating its promising application in a hostile nuclear environment.

Author Contributions: Investigation, J.Z.; Methodology, Y.Z.; Project administration, Y.Z.; Writing—original draft, J.Z. and Y.Z.; Writing—review & editing, Y.L. All authors have read and agreed to the published version of the manuscript.

Funding: This work was supported by the National Basic Research Program of China (973 program, No. 2013CB035505), and the Fundamental Research Funds for the Central Universities (50321041917001).

Conflicts of Interest: The authors declare no conflict of interest.

References

1. Davis, W.K. Nuclear energy for the United States. *Energy* **1979**, *4*, 1053–1062. [[CrossRef](#)]
2. Chang, Y.C.; Zhao, Y. The Fukushima Nuclear Power Station incident and marine pollution. *Mar. Pollut. Bull.* **2012**, *64*, 897–901. [[CrossRef](#)] [[PubMed](#)]
3. Smith, J.T.; Comans, R.N.J.; Beresford, N.A.; Wright, S.M.; Camplin, W.C.; Howard, B.J. Pollution: Chernobyl's legacy in food and water. *Nature* **2000**, *405*, 141. [[CrossRef](#)] [[PubMed](#)]
4. Roger, J.L.; Nicole, F.D.S.; Henson, B.L. Incidence of thyroid cancer surrounding three mile island nuclear facility: The 30-year follow-up. *Laryngoscope* **2013**, *123*, 2064–2071.
5. Komarneni, S.; Roy, R. Alternative radwaste solidification route for three mile island wastes. *J. Am. Ceram. Soc.* **1982**, *65*, C198. [[CrossRef](#)]
6. Hlgye, Z.; Malátová, I. Estimation of intakes of ^{131}I , ^{137}Cs and ^{134}Cs after the Chernobyl accident. *Radiat. Prot. Dosim.* **2012**, *150*, 504–507. [[CrossRef](#)]
7. Chino, M.; Nakayama, H.; Nagai, H.; Terada, H.; Katata, G. Preliminary estimation of release amounts of ^{131}I and ^{137}Cs accidentally discharged from the Fukushima Daiichi Nuclear Power Plant into the atmosphere. *J. Nucl. Sci. Technol.* **2011**, *48*, 1129–1134. [[CrossRef](#)]
8. EL-Zayat, M.M.; Abdel-Hakim, A.; Mohamed, M.A. Effect of gamma radiation on the physico mechanical properties of recycled HDPE/modified sugarcane bagasse composite. *J. Macromol. Sci. Part A* **2019**, *56*, 127–135. [[CrossRef](#)]
9. Liu, G.; Liu, H.; Liu, Y.; He, S. The degradation of DGEBA/DICY under 100 keV proton irradiation. *Polym. Degrad. Stab.* **2011**, *96*, 732–738. [[CrossRef](#)]
10. Yamamoto, M.; Nishikawa, N.; Mayama, H.; Nonomura, Y.; Yokojima, S.; Nakamura, S.; Uchida, K. Theoretical explanation of the lotus effect: Superhydrophobic property changes by removal of nanostructures from the surface of a lotus leaf. *Langmuir* **2015**, *31*, 7355–7363. [[CrossRef](#)]
11. Yoon, Y.; Kim, D.; Lee, J.B. Hierarchical micro/nano structures for super-hydrophobic surfaces and super-lyophobic surface against liquid metal. *Micro Nano Syst. Lett.* **2014**, *2*, 3. [[CrossRef](#)]
12. Bixler, G.D.; Bhushan, B. Bioinspired rice leaf and butterfly wing surface structures combining shark skin and lotus effects. *Soft Matter* **2012**, *8*, 11271–11284. [[CrossRef](#)]
13. Wang, F.; Li, S.; Wang, L. Fabrication of artificial super-hydrophobic lotus-leaf-like bamboo surfaces through soft lithography. *Colloids Surf. A* **2017**, *513*, 389–395. [[CrossRef](#)]
14. Hardman, S.J.; Muhamad-Sarih, N.; Riggs, H.J.; Thompson, R.L.; Rigby, J.; Bergius, W.N.A.; Hutchings, L.R. Electrospinning superhydrophobic fibers using surface segregating end-functionalized polymer additives. *Macromolecules* **2011**, *44*, 6461–6470. [[CrossRef](#)]
15. Zander, N.E.; Orlicki, J.A.; Karikari, A.S.; Long, T.E.; Rawlett, A.M. Super-Hydrophobic surfaces via micrometer-scale templated pillars. *Chem. Mater.* **2007**, *19*, 6145–6149. [[CrossRef](#)]
16. Farzaneh, M.; Menini, R.; Jafari, R. Superhydrophobic and icephobic surfaces prepared by RF-sputtered polytetrafluoroethylene coatings. *Appl. Surf. Sci.* **2010**, *257*, 1540–1543.
17. He, G.; Kaige, W. The super hydrophobicity of ZnO nanorods fabricated by electrochemical deposition method. *Appl. Surf. Sci.* **2011**, *257*, 6590–6594. [[CrossRef](#)]
18. Shieh, J.; Hou, F.J.; Chen, Y.C.; Chen, H.M.; Yang, S.P.; Cheng, C.C.; Chen, H.L. Robust airlike superhydrophobic surfaces. *Adv. Mater.* **2010**, *22*, 597–601. [[CrossRef](#)]
19. Ren, L.F.; Xia, F.; Shao, J.; Zhang, X.; Li, J. Experimental investigation of the effect of electrospinning parameters on properties of superhydrophobic PDMS/PMMA membrane and its application in membrane distillation. *Desalination* **2017**, *404*, 155–166. [[CrossRef](#)]
20. Lu, Y.; Sathasivam, S.; Song, J.; Crick, C.R.; Carmalt, C.J.; Parkin, I.P. Robust self-cleaning surfaces that function when exposed to either air or oil. *Science* **2015**, *347*, 1132–1135. [[CrossRef](#)]
21. Jiangab, T.; Guoab, Z. Robust superhydrophobic tungsten oxide coatings with photochromism and UV durability properties. *Appl. Surf. Sci.* **2016**, *387*, 412–418. [[CrossRef](#)]
22. Pintoa, D.; Bernardob, L.; Amaroa, A.; Lopesa, S. Mechanical properties of epoxy nanocomposites using titanium dioxide as reinforcement—A review. *Constr. Build. Mater.* **2015**, *95*, 506–524. [[CrossRef](#)]
23. Xia, W.; Xue, H.; Wang, J.; Wang, T.; Song, L.; Guo, H.; Fan, X.; Gong, H.; He, J. Functionalized graphene serving as free radical scavenger and corrosion protection in gamma-irradiated epoxy composites. *Carbon* **2016**, *101*, 315–323. [[CrossRef](#)]

24. Li, R.; Gu, Y.; Wang, Y.; Yang, Z.; Li, M.; Zhang, Z. Effect of particle size on gamma radiation shielding property of gadolinium oxide dispersed epoxy resin matrix composite. *Mater. Res. Express* **2017**, *4*, 035035. [[CrossRef](#)]
25. Chang, L.; Zhang, Y.; Liu, Y.; Fang, J.; Luan, W.; Yang, X.; Zhang, W. Preparation and characterization of tungsten/epoxy composites for γ -rays radiation shielding. *Nucl. Instrum. Methods Phys. Res. Sect. B* **2015**, *356–357*, 88–93. [[CrossRef](#)]
26. Nagatani, K.; Kiribayashi, S.; Okada, Y.; Otake, K.; Yoshida, K.; Tadokoro, S.; Nishimura, T.; Yoshida, T.; Koyanagi, E.; Fukushima, M.; et al. Emergency response to the nuclear accident at the Fukushima Daiichi Nuclear Power Plants using mobile rescue robots. *J. Field Robot.* **2013**, *30*, 44–63. [[CrossRef](#)]
27. Stöber, W.; Fink, A.; Bohn, E. Controlled growth of monodisperse silica spheres in the micron size range. *J. Colloid Interface Sci.* **1968**, *26*, 62–69. [[CrossRef](#)]
28. GB/T 1677–2008 *Determinating the Epoxy Value of Plasticizers*; SAC: Beijing, China, 2008.
29. D3359-09 *Standard Test Methods for Measuring Adhesion by Tape Test*; ASTM: West Conshohocken, PA, USA, 2009.
30. D3363-00 *Standard Test Method for Film Hardness by Pencil Test*; ASTM: West Conshohocken, PA, USA, 2000.
31. Gao, Y.Y.; Zhang, Z.L.; Chen, W.X. Several dose meters for radiation processing—the first intercomparison held in Beijing. *J. Rad. Res. Rad. Proc.* **1988**, *6*, 37–41.
32. Ming, W.; Wu, D.; van Benthem, R.; de With, G. Superhydrophobic films from raspberry-like particles. *Nano Lett.* **2005**, *5*, 2298–2301. [[CrossRef](#)]
33. Pureskiy, N.; Ionov, L. Synthesis of robust raspberry-like particles using polymer brushes. *Langmuir* **2011**, *27*, 3006–3011. [[CrossRef](#)]
34. Wang, C.F.; Hung, S.W.; Kuo, S.W.; Chang, C.J. Combining hierarchical surface roughness with fluorinated surface chemistry to preserve superhydrophobicity after organic contamination. *Appl. Surf. Sci.* **2014**, *320*, 658–663. [[CrossRef](#)]
35. Li, F.; Du, M.; Zheng, Q. Dopamine/Silica nanoparticle assembled, microscale porous structure for versatile superamphiphobic coating. *ACS Nano* **2016**, *10*, 2910–2921. [[CrossRef](#)]
36. Yang, J.; Pi, P.; Wen, X.; Zheng, D.; Xu, M.; Cheng, J.; Yang, Z. A novel method to fabricate superhydrophobic surfaces based on well-defined mulberry-like particles and self-assembly of polydimethylsiloxane. *Appl. Surf. Sci.* **2009**, *255*, 3507–3512. [[CrossRef](#)]
37. Bobji, M.S.; Kumar, S.V.; Asthana, A.; Govardhan, R.N. Underwater sustainability of the “Cassie” state of wetting. *Langmuir* **2009**, *25*, 12120–12126. [[CrossRef](#)] [[PubMed](#)]
38. Latthe, S.S.; Sutar, R.S.; Bhosale, A.K.; Nagappan, S.; Ha, C.S.; Sadasivuni, K.K.; Liu, S.; Xing, R. Recent developments in air-trapped superhydrophobic and liquid-infused slippery surfaces for anti-icing application. *Prog. Org. Coat.* **2019**, *137*, 1–17. [[CrossRef](#)]
39. Lee, S.G.; Ham, D.S.; Lee, D.Y.; Bong, H.; Cho, K. Transparent superhydrophobic/translucent superamphiphobic coatings based on silica-fluoropolymer hybrid nanoparticles. *Langmuir* **2013**, *29*, 15051–15057. [[CrossRef](#)] [[PubMed](#)]
40. Vignoud, L.; Sixou, B.; David, L. Influence of electron irradiation on the mobility and on the mechanical properties of DGEBA/TETA epoxy resins. *Polymer* **2001**, *42*, 4657–4665. [[CrossRef](#)]
41. Diao, F.; Zhang, Y.; Liu, Y.; Fang, J.; Luan, W. γ -Ray irradiation stability and damage mechanism of glycidyl amine epoxy resin. *Nucl. Instrum. Methods Phys. Res. Sect. B* **2016**, *383*, 227–233. [[CrossRef](#)]
42. Qi, Y.; Ping, C.; Gao, Y.; Ma, K.; Chun, L.; Xuhuai, X. Effects of electron irradiation in space environment on thermal and mechanical properties of carbon fiber/bismaleimide composite. *Nucl. Instrum. Methods Phys. Res. Sect. B* **2014**, *336*, 158–162.

